AIAA'85

AIAA-85-0491

The Görtler Instability on an Airfoil

S. M. Mangalam
Old Dominion University
Hampton, VA 23665

J. R. Dagenhart
NASA Langley Research Center
Hampton, VA 23665

T. E. Hepner
United States Army (AVRADCOM)
Hampton, VA 23665

and

J. F. Meyers
NASA Langley Research Center
Hampton, VA 23665

AIAA 23rd Aerodynamic Sciences Meeting

January 14-17, 1985/ Reno, Nevada

The Görtler Instability on an Airfoil

S. M. Mangalam*
Old Dominion University
Norfolk, Virginia 23508

J. R. Dagenhart**
NASA Langley Research Center
Hampton, Virginia 23665

T. E. Hepner***
United States Army (AVRADCOM)
Hampton, Virginia 23665

J. F. Meyers****
NASA Langley Research Center
Hampton, Virginia 23665

Abstract

Görtler vortices arise in boundary layers along concave surfaces due to centrifugal effects. This paper presents some results of an experiment conducted to study the development of these vortices on an airfoil with a pressure gradient in the concave region where an attached laminar boundary layer was insured with suction through a perforated panel. The sublimating chemical technique was used to visualize Görtler vortices and the velocity field was measured by laser velocimetry. The vortex wavelength clearly varied with Görtler number as predicted by linear theory. Both flow visualization and velocity measurements indicated vortex damping in the convex zone. Secondary instability was observed at the higher Görtler numbers.

---

* Research Associate Professor, Member AIAA
** Aerospace Engineer, Transonic Aerodynamics Division
*** Electronic Technician, Instrument Research Division
**** Electronic Engineer, Instrument Research Division

Symbols

C_p	pressure coefficient
c	chord length
$G \quad \frac{U \ \delta_r}{\nu} \sqrt{\frac{\delta_r}{r}}$	Görtler number
G_M	Görtler number at maximum curvature
M_∞	free-stream Mach number
R_c	Reynolds number based on chord
$R' \quad \frac{U}{\nu}$	unit Reynolds number
r	radius of curvature
U_∞	free-stream velocity
U, V, W	velocity components in laser coordinates
u	streamwise boundary-layer velocity component
x, y, z	model coordinates
α	wave number
$\delta_r \quad \sqrt{\frac{\nu X}{U}}$	boundary layer thickness parameter
$\Lambda \quad \frac{}{\nu} \ \bar{\lambda}$	nondimensional wavelength

Introduction

Görtler vortices arise in boundary layers along concave surfaces due to centrifugal effects. These counter-rotating streamwise vortices are one of three known flow instabilities which lead to boundary layer transition. Coupled with Tollmien-Schlichting waves and crossflow vortices these Görtler vortices can trigger early transition to

turbulence. Görtler vortices may play an important role in internal flows with concave curvature and on modern supercritical laminar-flow-control wings which have concave regions near the leading and trailing edges of the lower surfaces.

This centrifugal instability was first treated analytically by Görtier[1] after whom the vortices are named. The stability is governed by the parameter

$$G \quad \frac{U \ \delta_r}{\nu} \sqrt{\frac{\delta_r}{r}}$$

where δ_r is a suitable boundary layer thickness, r is the radius of curvature, and ν is the fluid kinematic viscosity. Many studies have since been devoted to the improvement and extension of Görtler's analysis and a thorough survey of these efforts has been reported by Herbert.[2] There are a number of fundamental differences in these theoretical studies as to the details of the formulation of the problem as well as in the computed results. These are discussed in Floryan's thesis.[3] The influence of external disturbances is analyzed by Floryan and Saric[4] and the influence of pressure gradient is discussed by Hall.[5]

There have also been a number of experimental studies of this problem, mostly conducted in curved channel flows. Tani *et al*,[6-9] attempted to correlate the streamwise vortex wavelength with wall curvature and free stream velocity (i.e., Görtler number) as predicted by theory. The failure to find such a correlation led them to the conclusion that the vortex wavelength is determined more by the particular edge effects of the experimental apparatus and less by the curvature of the model or the velocity of the oncoming flow. Several other experimenters including Bippes,[10] McCormack *et al*,[11] Winto *et al*,[12] Yurchenco *et al*,[13] Babenko[14] and Yurchenco[15], and Swearingen and Blackwelder[16] have also found that the wavelength is essentially independent of the Görtler number. Bippes[10] did find that when the stream turbulence was made isotropic, the most amplified disturbance according to theory could be generated. Experimental data from these studies seem to indicate that some preferred wave number disturbance is selected initially from those unstable ones and is amplified with increasing Görtler number while roughly following lines of constant

$$\Lambda \quad \frac{U \ r}{\nu} \ \frac{\lambda}{r}^{\frac{3}{2}}$$

where λ is the wavelength. The present paper evaluates this parameter on the basis of tests conducted on a two-dimensional airfoil model.

Results from flow visualization tests using sublimating chemicals and laser velocimeter measurements are compared.

Test Apparatus

A 1.83-meter chord airfoil model was tested in the NASA Langley Low-Turbulence Pressure Tunnel (LTPT). A photograph of the model is shown in figure 1 . The model consists of two parts a structural element and a test element. The test element includes the leading edge and the upper surface back to midchord. The structural element consists of the spar and the remainder of the airfoil surface including a 10% chord flap. With this design, several test region geometries can be examined. The present test element includes a concave region from $x/c = 0.175$ to $x/c = 0.275$. The minimum radius of curvature is 0.24 m. Attached laminar boundary-layer flow is insured by means of suction through a 0.11 x 0.76-m perforated titanium panel located in the compression part of the concave region. The suction region is divided into three spanwise suction strips. The suction in each strip is independently controlled by its own needle valve. The model surface is painted flat black over gel coat and fiberglass. Figure 2 shows the model pressure distribution. The 10% chord flap is used to control the stagnation point location to maintain a flat or slightly favorable pressure gradient ahead of the concave region.

The LTPT is a pressurized, closed-circuit, continuous flow wind tunnel. The test section is 2.29 m high, 2.29 m long, and 0.91m wide. The contraction ratio is 17.6. The tunnel has excellent flow quality due, in part, to the nine screens in the settling chamber. The velocity fluctuations in the test section were found to be 0.025 percent at 0.05 Mach number.[1] The pressure fluctuations at the test section wall, normalized with respect to free-stream pressure were 10^{-5} at this Mach number.

The present experiment was conducted at atmospheric pressure. The chord Reynolds number was varied from 1.0 million to 5.9 million and the Mach number ranged from 0.024 to 0.125 yielding a Görtler number of up to 46.

A specialized single axis three-component laser velocimeter was used to study the flow field in the test region (fig. 3). The single axis, five-beam optical configuration[1] uses the standard two color, two-component beam pattern with the two green beams (514.5 nm) arranged in the horizontal plane and the two blue beams (488.0 nm) arranged in the vertical plane forming a diamond pattern to measure the U or streamwise component (green beams) and the V or vertical

component (blue beams). A third green beam is placed along the optical axis bisecting the angle between the original two green beams. The addition of this beam creates two additional fringe patterns within the sample volume. These additional fringe patterns are inclined symmetrically about the optical axis yielding equal contributions of the U component and equal but opposite contributions of the W or spanwise velocity component. The W velocity component is then obtained from the difference between the two signal frequencies. This is achieved by incorporating Bragg cells in the two outside beams to separate by frequency the three signals obtained from the three green fringe patterns. A filter network isolates the U component signal frequency and the two signal frequencies from the inclined fringe patterns which are then input to an electronic double balanced mixer. The lower frequency signal from the mixer is the frequency difference between the two input signals and is the W component signal frequency with a known bias depending on Bragg cell frequencies. The flow was seeded with tridecane particles using a particle generator located upstream of the settling chamber screens. The LV data were recorded and processed by a dedicated computer system. The velocity components were measured in the laser velocimeter coordinate system which looked down on the model at an angle of 11 . These velocity components were then transformed into wind-tunnel and model coordinate systems for analysis.

Results and Discussion

A thin layer of solid white biphenyl material was sprayed over the black model surface to visualize the flow. This hydrocarbon material sublimes due to the heat transfer at the airfoil surface which is proportional to the surface shear stress[19]. The flow pattern is made visible due to the differential surface shear stress distribution under the layer of counter-rotating Görtler vortices. Elapsed times of about 30 minutes to 1 hour were required for the pattern to emerge clearly, depending on the free-stream velocity. Representative flow patterns are shown in Figures 4 (a), (b), and (c) taken at chord Reynolds numbers of 2.24, 3.21, and 3.67 million respectively. The dark bands represent the high shear stress regions where the chemical layer has sublimated revealing the black background of the airfoil surface, whereas, the white bands correspond to low shear regions. A set of black and white bands constitutes a pair of counter-rotating vortices and represents the wavelength of these vortices.

The photographs in figure 4 show the region $0.20 < x/c < 0.40$ near the center of the model span. The perforated titanium suction panel is visible at the upstream edge of each photograph. No streamwise

streaks were observed in the region ahead of the concave zone. The streaks observed downstream of the suction panel are essentially uniformly spaced along the span. Wavelength was determined by taking the average of the number of pairs of streaks over a 15 to 45 cm span. The nondimensional wavelength parameter Λ was computed using this value of dimensional wavelength and the mean flow and geometric parameters. The dimensional wavelength appears to remain constant throughout the concave region. Beyond the concave region the streaks decrease considerably in contrast but remain visible back to the jagged transition line. This indicates damping of the Görtler vortices in the convex region which is confirmed by the laser velocimeter measurements discussed below. Furthermore, in the convex zone, occasional vortex mergers are visible.

Figures 5 and 6 show the variation of the streamwise velocity component along the span from 1.5 to 4.5 cm left of midspan at several heights above the model surface for chord Reynolds numbers of 1.0 and 2.1 million, respectively. These Reynolds numbers correspond to Mach numbers of 0.024 and 0.05. The measurements presented are for chord locations of x/c = 0.15, 0.175, 0.20, 0.225, 0.25, 0.275, 0.30, and 0.3375 for M_∞ = 0.05 and all of these except x/c = 0.15 for M_∞ = 0.024. The first and last of these locations are just ahead and aft of the concave zone, respectively. All three boundary-layer velocity components were measured, but only the streamwise boundary-layer component data are shown since this component is much larger than the other two. The spanwise scan lines for the higher Reynolds number data were taken in a vertical plane. The scanning method was later changed so that the scan lines for the lower Reynolds number data lie in a plane normal to the model surface. Figures 5 and 6 show a general decrease in velocity with increasing z. This is caused by minute deflections of the floor supporting the heavy laser optics traversing mechanism. The heights y indicated on the figure keys are correct at z = 1.5 cm. The maximum deflection of the laser control volume was measured to be Δy = 0.018 cm. The concave region of the model begins at x/c = 0.175. However, figures 5(a), 6(a), and 6(b) show small, but definite, periodic velocity variations along the span at x/c = 0.175. The disturbance wavelength was determined by direct examination of the streamwise velocity plots and by examination of the autocovariance function determined using the Fast Fourier Transform (FFT) technique.

For G_M = 29.9, figure 5(d) shows that the periodic velocity pattern is well developed by x/c = 0.25. The increase of the disturbance amplitude from x/c = 0.175 to 0.275 is clearly evident (figs. 5(a) - (e)). In the convex zone beyond x/c = 0.275, the disturbance amplitude decreases (fig. 5(f) and 5(g)). The dimensional disturbance wavelength remains essentially constant at λ = 0.6 cm throughout the measurement range

at all heights except possibly near the boundary-layer edge at x/c = 0.275 where a doubling or tripling of the wavelength may be beginning.

For G_M = 36.0, the disturbance velocity pattern is more complex. Periodic spanwise variations are clearly evident from x/c = 0.15, (fig. 6(a)) and are well developed at the lower levels of the boundary layer by x/c = 0.225 (fig. 6(d)). However, a strong secondary disturbance with wavelength 4 to 5 times that of the basic instability abruptly appears at x/c = 0.225 (fig. 6(d)). The maximum velocity difference reaches sixty percent of the local edge velocity for y = 0.2 cm (fig. 6(d)). This secondary instability has been noted before by Wortman[20] and Bippes[10]. The secondary disturbance decays markedly in the accelerated flow region beyond x/c = 0.225 and the following convex region (fig. 6(d)-6(h)). Visual examination of the velocity plots and the autocovariance functions for the data of figure 6 indicate a disturbance wavelength of λ = 0.3 cm. This wavelength is clearly evident from x/c = 0.225 to 0.30. At x/c = 0.3375, the dominant wavelength appears to be λ = 0.6 cm or twice the basic wavelength; however, the autocovariance functions for this data indicate that variations of the shorter wavelength are still present.

Laser velocimeter measurements of streamwise velocity at all chord locations as well as at all heights above the surface were used to determine disturbance wavelength, using autocovariance function. Except where secondary instability was present, the wavelength did not vary by more than 10% throughout the measurement zone at a given free stream condition. Wavelengths, determined from laser measurements, agree well with those observed in flow visualization. As in all previous experiments, the dimensional wavelength of the disturbance was conserved in the flow direction but unlike earlier experiments the wavelength was observed to vary appreciably with free stream conditions. The variation in wavelength was most noticeable at lower speeds as seen from figure 7 where λ is plotted against Görtler number. The theoretical curve corresponds to wavelength computed from maximum amplification conditions.[3] It is seen that experimental values of λ lie very close to wavelengths predicted on the basis of linear theory. The nondimensional wavelength parameter Λ obtained from flow visualization and laser velocimeter measurements is also shown plotted as a function of Görtler number G_M in figure 8 where it is compared with existing experimental data and Floryan's[3] theoretical results.

Conclusions

1. A fixed, essentially uniform, vortex spacing was observed in the concave zone by both flow visualization and laser velocimeter measurements for each flow condition.

2. Both flow visualization and laser velocimeter measurements show a vortex wavelength which varied with Görtler number in accordance with linear stability theory.

3. A significant, abrupt decrease in streak contrast indicated vortex damping in the convex zone.

4. The velocity measurements showed both disturbance amplification in the concave zone and damping in the following convex zone.

5. Flow visualization did not indicate a vortex pattern ahead of the concave zone; however, velocity measurements indicated small spanwise variations of the streamwise velocity component at or just ahead of the beginning of the concave zone. The wavelength of this variation matched the observed wavelength in the downstream concave region.

6. The flow visualization showed some apparent vortex mergers in the convex zone.

7. The velocity measurements indicated a stationary secondary instability in the concave zone.

Acknowledgments

This research was initiated when the first author was a Research Associate in the National Research Council Associateship Program. The authors wish to sincerely thank W. Pfenninger and W. D. Harvey for their useful comments and discussions at various stages of the experiment.

References

1. Görtler, H.: *Instabilitat laminaren Grenzchichten an konkaven Wanden gegeniiber gewissen dreidimensionalen Storungen*. ZAMM Vol. 21., No. 1, 1941, pp. 250-252.

2. Herbert, Th.: *On the stability of the boundary layer along a concave wall*. Arch. Mechaniki Stosowanej, Vol. 28, No. 5-6, 1976, pp. 1039-1055.

3. Floryan, J. M.: *Stability of Boundary-Layer Flows over Curved Walls*. Ph.D. Thesis, Virginia Polytechnic Institute and State University, Blacksburg, VA., Jan. 1980.

4. Floryan, H. M. and Saric, W. S.: *Stability of Görtler Vortices in Boundary Layers*. AIAA J., Vol. 20, No. 3, March 1983, pp. 316-324.

5. Hall, P.: *The Linear Development of Görtler Vortices in Growing Boundary Layer*. J. Fluid Mech., Vol. 30, 1983, pp. 41-58.

6. Tani, I.: *Some Aspects of Boundary-Layer Transition at Subsonic Speeds*. Advances In Aeronautical Sciences, Vol. 3, 1961, pp. 143-160.

7. Tani, I.: *Prediction of Longitudinal Vortices in the Boundary Layer Along a Curved Wall*. J. Geophys. Res., Vol. 67, 1962, pp. 3075-3080.

8. Tani, I. and Aihara, Y.: *Görtler Vortices and Boundary-Layer Transition*. ZAMP, Vol. 20, 1969, pp. 609-618.

9. Tani, I. and Sakagami, J.: *Boundary-Layer Instability at Subsonic Speeds*. Proc.ICAS, Third Congress, Stockholm, 1962, pp. 391-403.

10. Bippes, H.: *Experimental Study of the Laminar-Turbulent Transition on a Concave Wall in a Parallel Flow*. NASA TM 75243, 1978.

11. McCormack, P. D., *et al*: *Taylor-Görtler Vortices and Their Effect on Heat Transfer*. J. Heat Transfer, Trans. ASME, Feb. 1980, pp. 101-112.

12. Winoto, S. H., *et al*: *Measurements within Görtler Vortices*. J. Fluids Engineering, Trans. ASME, Vol. 101, 1979, pp. 517-520.

13. Yurchenko, N. F., *et al*: *Experimental Investigation of Görtler Instability in Boundary Layer*. in: Stratified and Turbulent Flows/in Russian/, Nauka Dumka, Kiev, 1979, pp. 50-59.

14. Babenko, V. V., and Yurchenko, N. F.: *Experimental Investigation of Görtler Instability on Rigid and Elastic Flat Plates*. Gidromekhanika, No. 41, 1980, pp. 103-108.

15. Yurchenko, N. F.: *Experimental Investigation of Streamwise Vortices in Boundary Layer*. Inzh. Fiz. Zhurnal, Vol. XLI, No. 6, December 1981, pp. 996-1002.

16. Swearingen, J. D. and Blackwelder, R. F.: *Parameters Controlling the Spacing of Streamwise Vortices on Concave Walls*. AIAA 21 Aerospace Sciences Meeting, Reno, Nevada, 1983. (AIAA-83-0380).

17. Stainback, P. C., and Owen, F. K.: *Dynamic Flow Quality Measurements in the Langley Low-Turbulence Pressure Tunnel*. Paper No. 84-0621, AIAA 13 Aerodynamic Testing Conference, San Diego, California, March 1984.

18. Meyers, J. F., and Hepner, T. E.: *Velocity Vector Analysis of a Juncture Flow Using a Three-Component Laser Velocimeter*. Second International Symposium on Applications of Laser Anemometry to Fluid Mechanics, July 2-4, 1984, Lisbon, Portugal.

19. Holmes, B. J., Croom, C. C., and Obara, C. J.: *Sublimating Chemical Method for Detecting Laminar Boundary-Layer Transition*. NASA Tech. Brief LAR-13089 (1982).

20. Wortman, F. X.: *Visualization of Transition*. J. Fluid Mech., Vol. 38, Part 3, 1969, pp. 473-480.

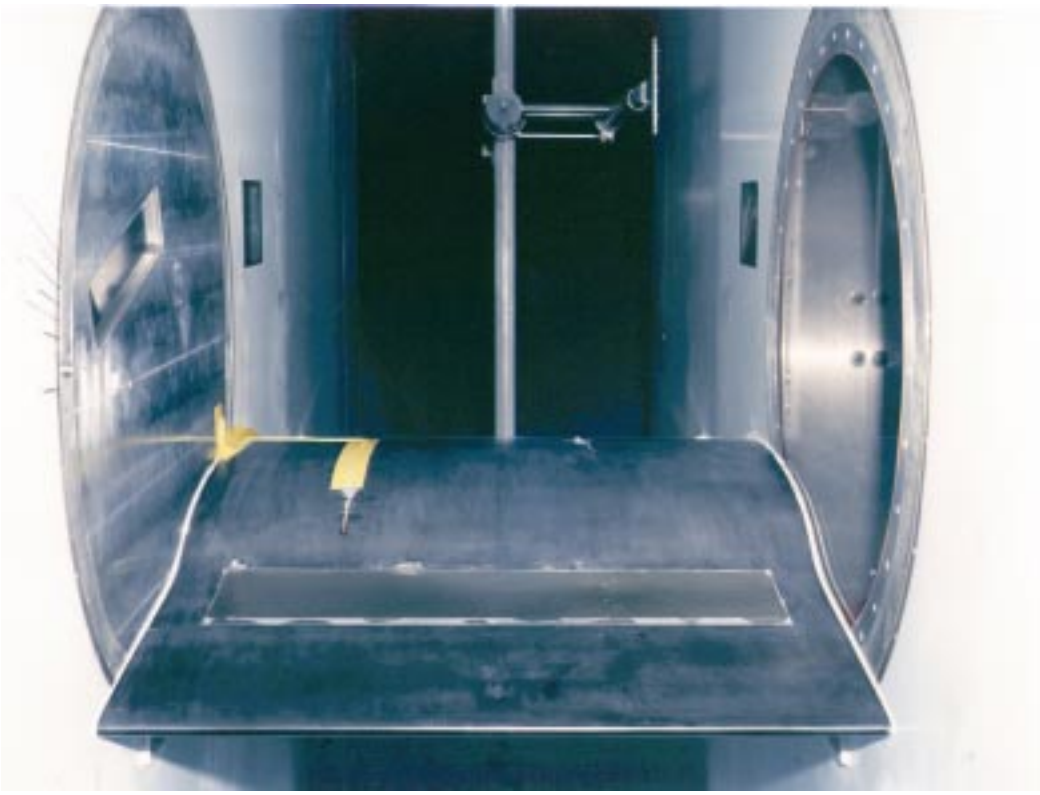

Figure 1.- Görtler model in LTPT.

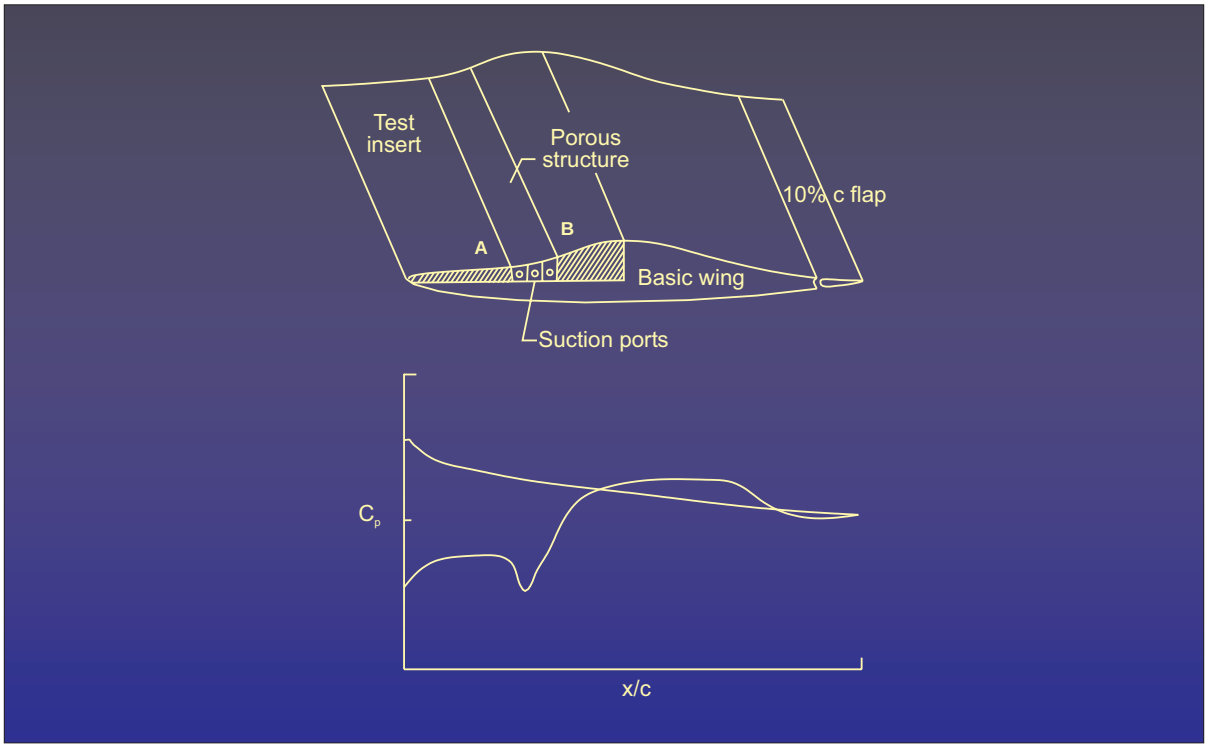

Figure 2.- Model schematic diagram and pressure distribution.

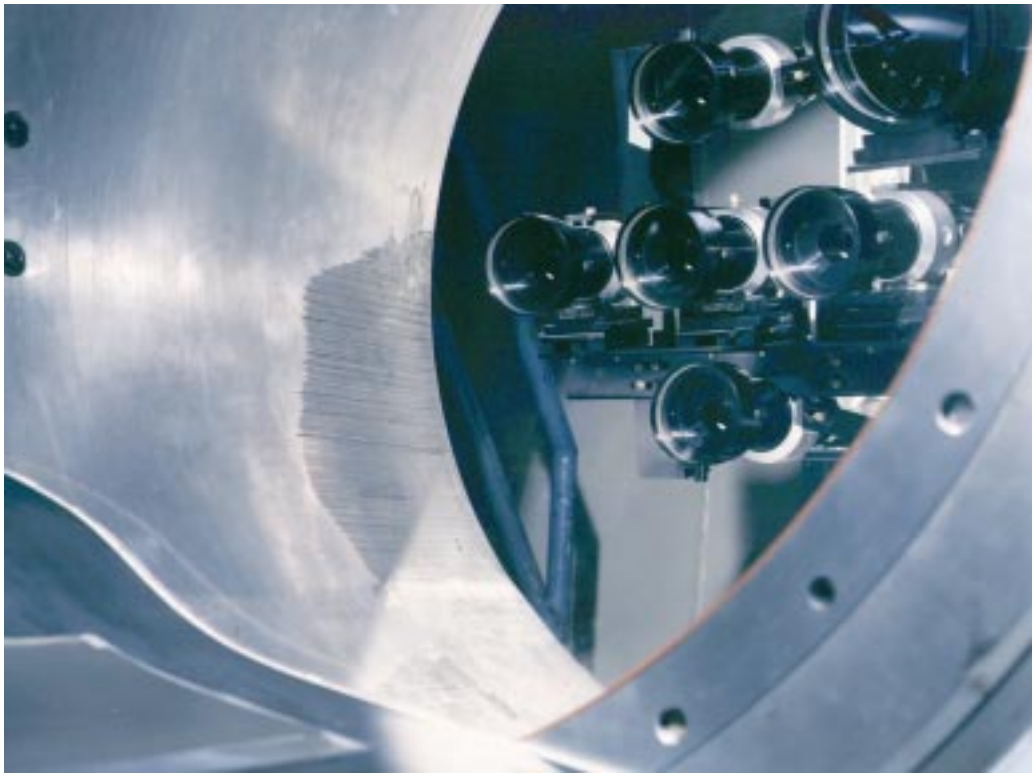

Figure 3.- Laser velocimeter optics.

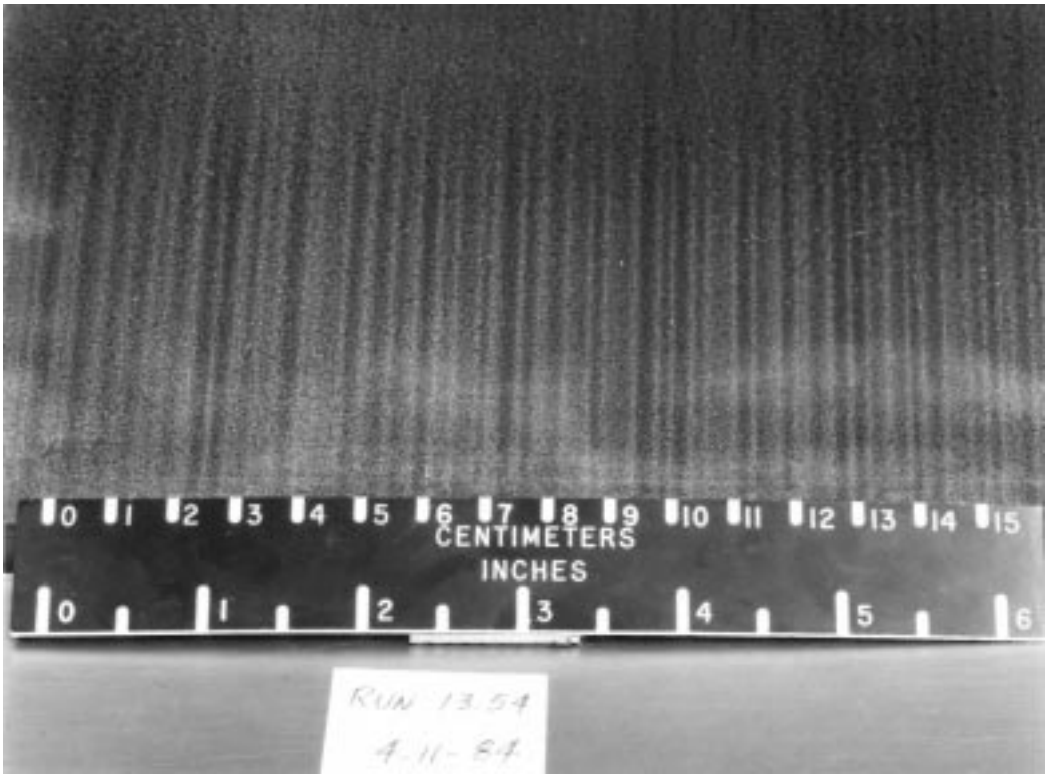

Figure 4(a).- Flow visualization using sublimating chemicals $M_\infty = 0.05$, $R_c = 2.24 \times 10^6$.

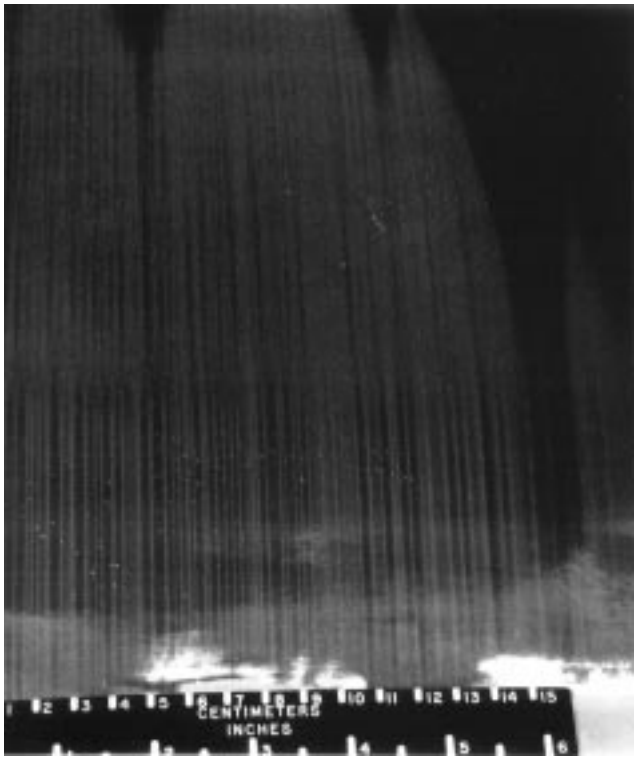

Figure 4(b).- Flow visualization using sublimating chemicals $M_\infty = 0.075$, $R_c = 3.21 \times 10^6$.

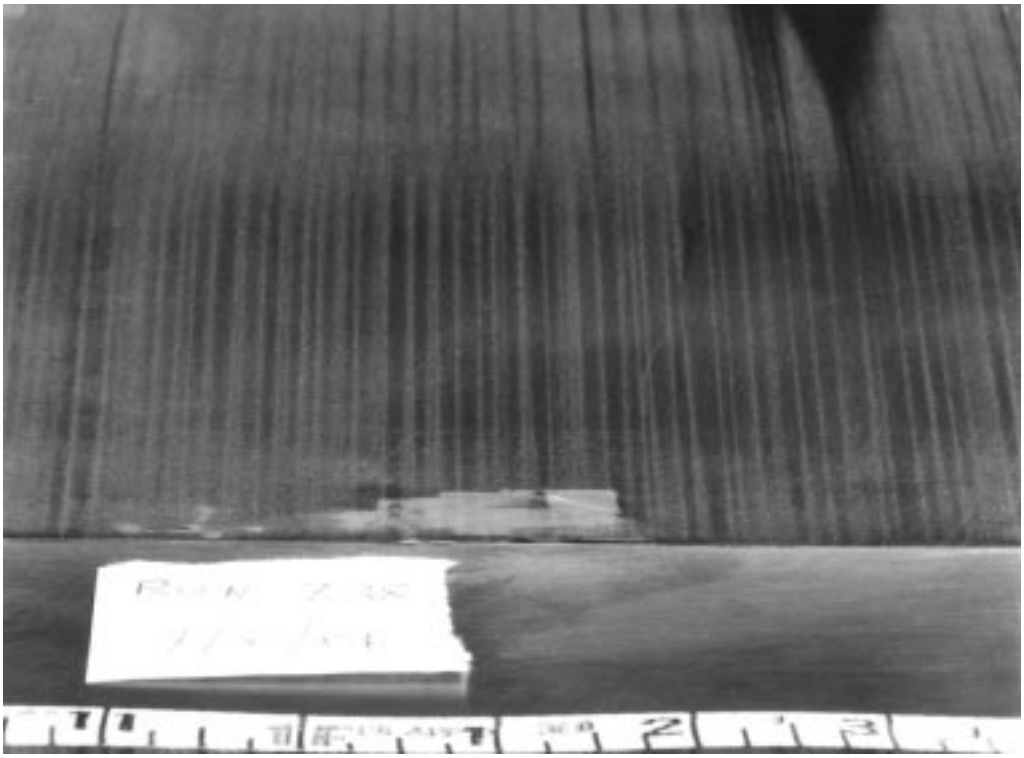

Figure 4(c).- Flow visualization using sublimating chemicals $M_\infty = 0.089$, $R_c = 3.67 \times 10^6$.

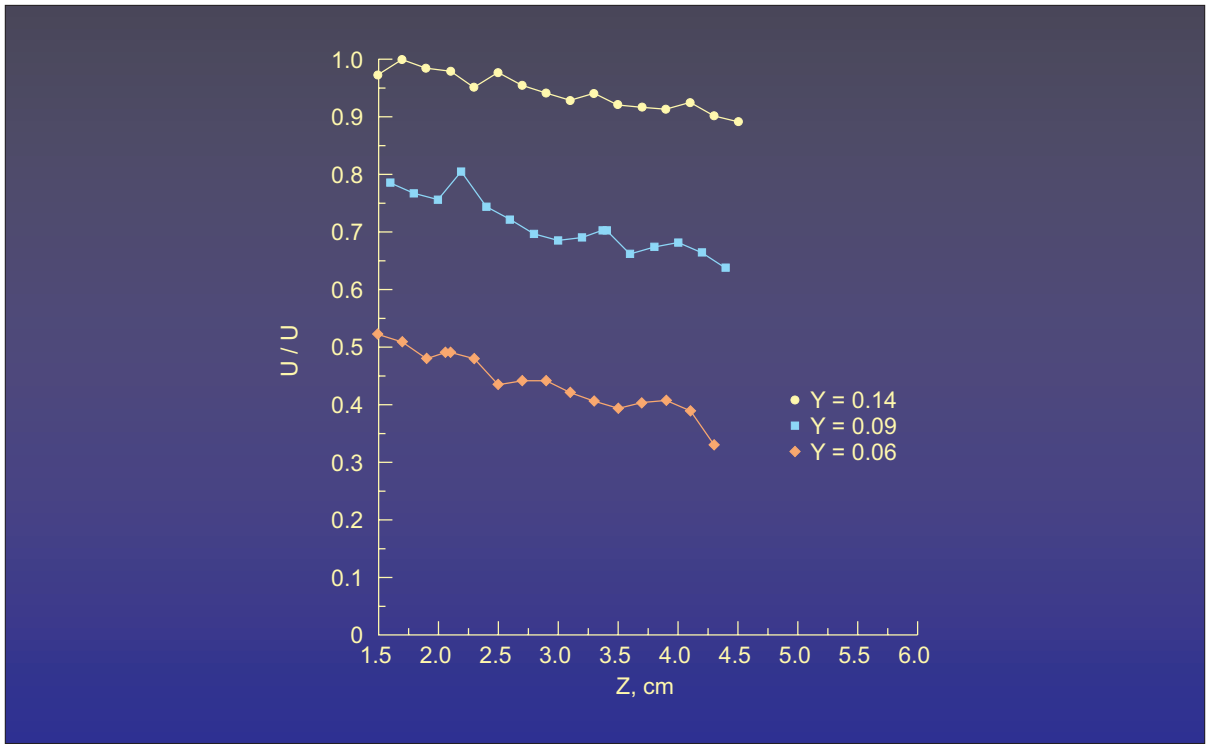

Figure 5(a).- Spanwise variation of streamwise velocity component $R_c = 1.0 \times 10^6$, $M_\infty = 0.024$, $G = 29.9$, $x/c = 0.175$.

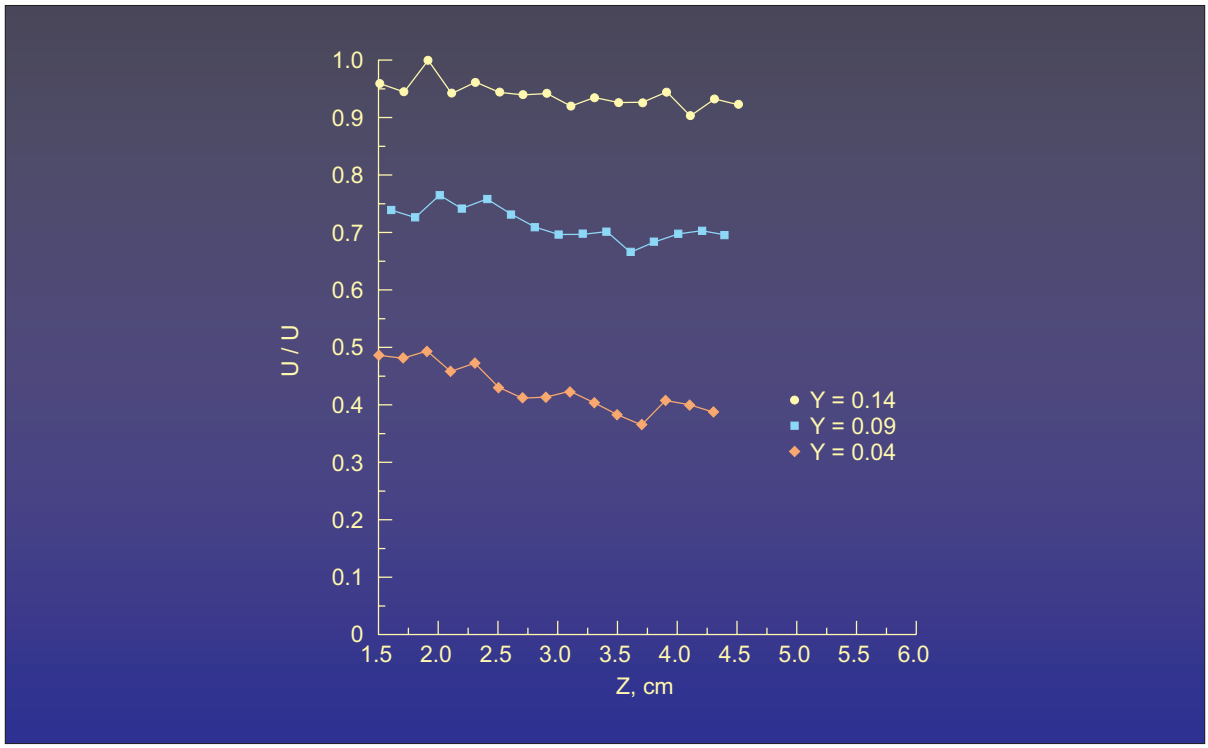

Figure 5(b).- Spanwise variation of streamwise velocity component $R_c = 1.0 \times 10^6$, $M_\infty = 0.024$, $G = 29.9$, $x/c = 0.20$.

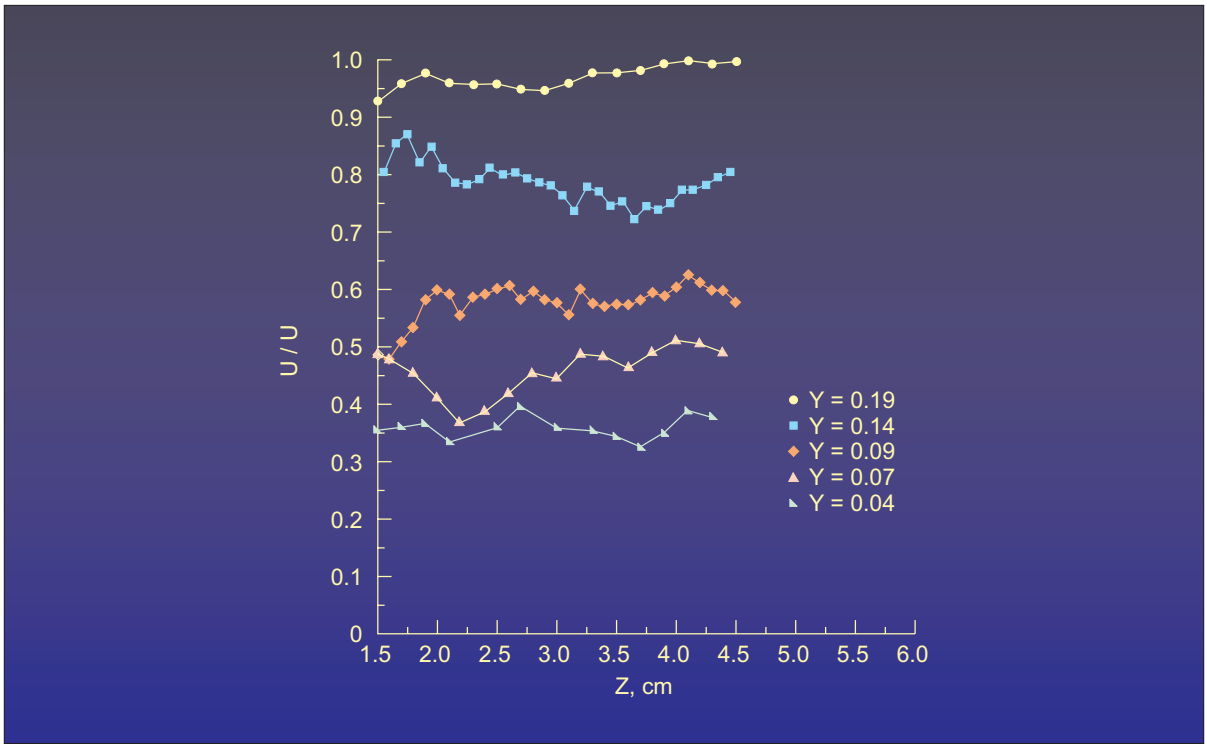

Figure 5(c).- Spanwise variation of streamwise velocity component $R_c = 1.0\text{x}10^6$, $M_\infty = 0.024$, $G = 29.9$, $x/c = 0.225$.

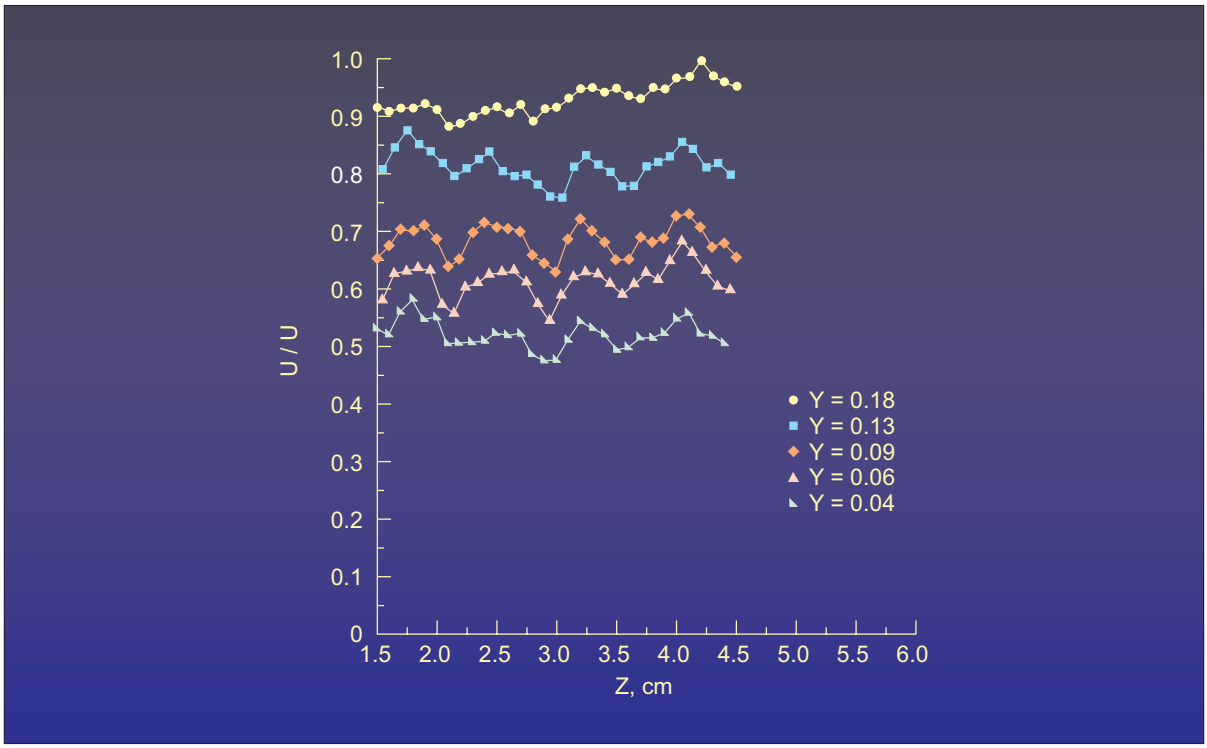

Figure 5(d).- Spanwise variation of streamwise velocity component $R_c = 1.0\text{x}10^6$, $M_\infty = 0.024$, $G = 29.9$, $x/c = 0.25$.

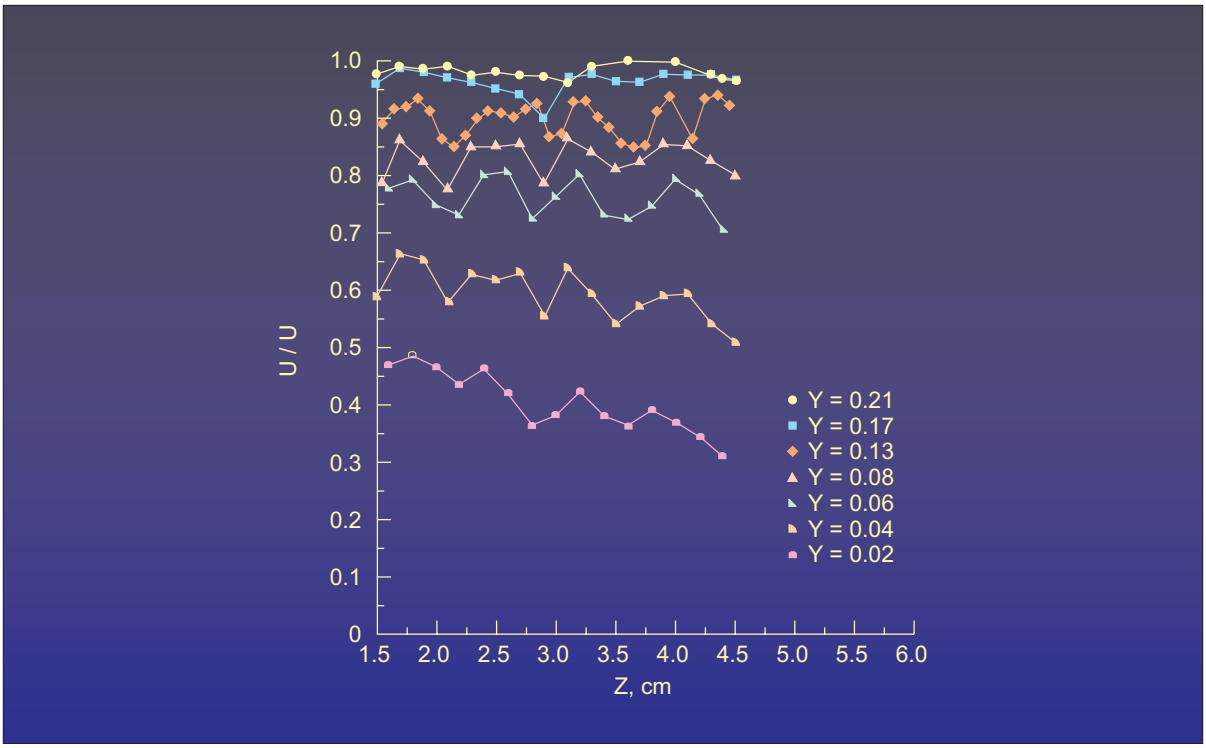

Figure 5(e).- Spanwise variation of streamwise velocity component $R_c = 1.0 \times 10^6$, $M_\infty = 0.024$, $G = 29.9$, $x/c = 0.275$.

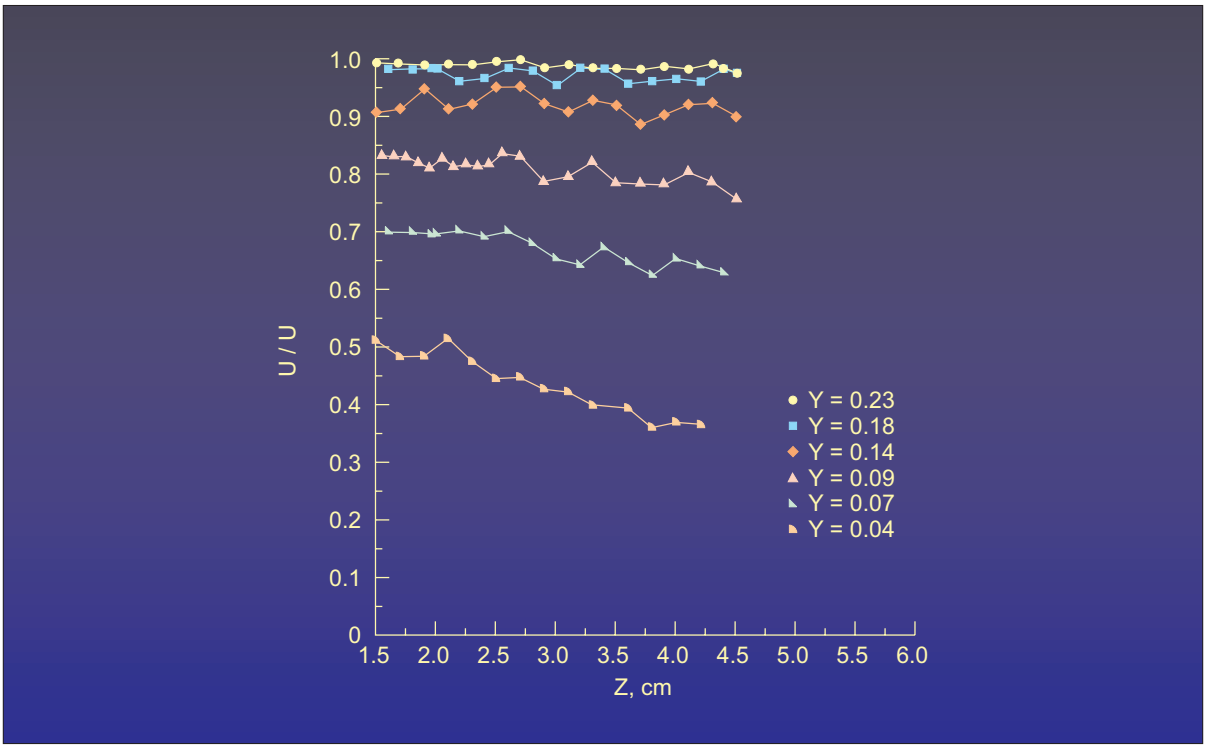

Figure 5(f).- Spanwise variation of streamwise velocity component $R_c = 1.0 \times 10^6$, $M_\infty = 0.024$, $G = 29.9$, $x/c = 0.30$.

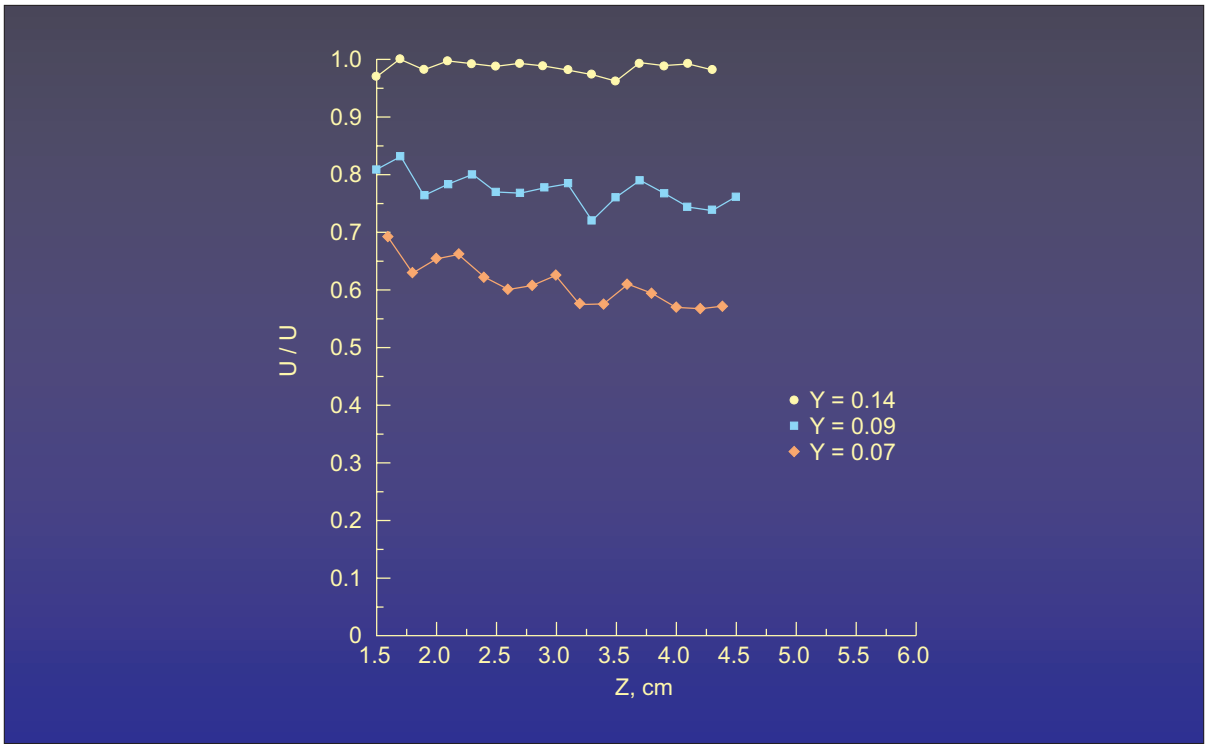

Figure 5(g).- Spanwise variation of streamwise velocity component $R_c = 1.0 \times 10^6$, $M_\infty = 0.024$, $G = 29.9$, $x/c = 0.3375$.

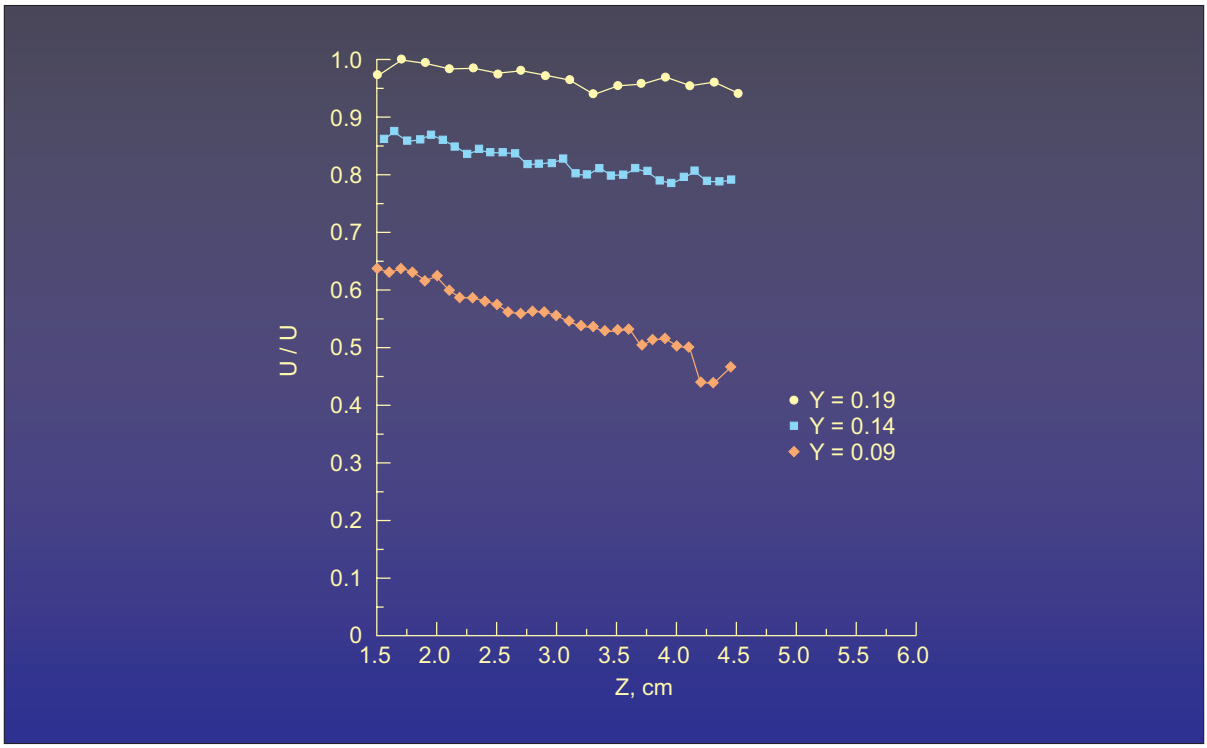

Figure 6(a).- Spanwise variation of streamwise velocity component $R_c = 2.1 \times 10^6$, $M_\infty = 0.05$, $G = 36.0$, $x/c = 0.15$.

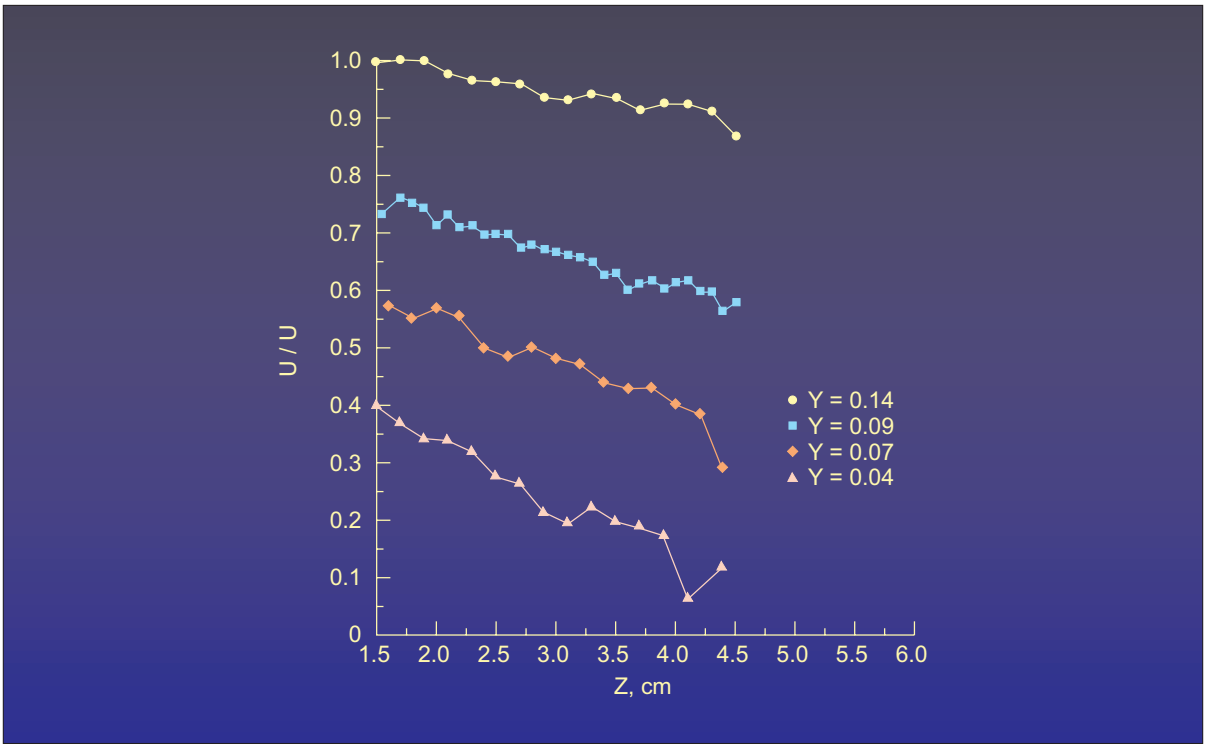

Figure 6(b).- Spanwise variation of streamwise velocity component $R_c = 2.1 \times 10^6$, $M_\infty = 0.05$, $G = 36.0$, $x/c = 0.175$.

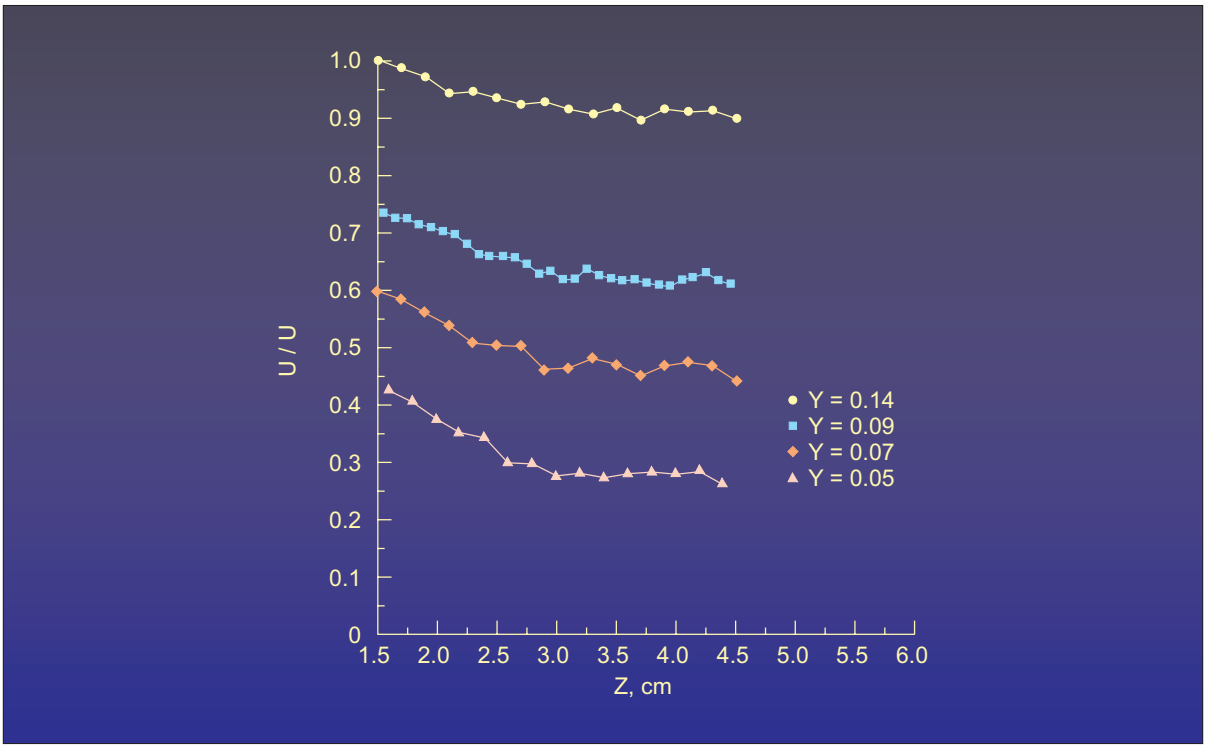

Figure 6(c).- Spanwise variation of streamwise velocity component $R_c = 2.1 \times 10^6$, $M_\infty = 0.05$, $G = 36.0$, $x/c = 0.20$.

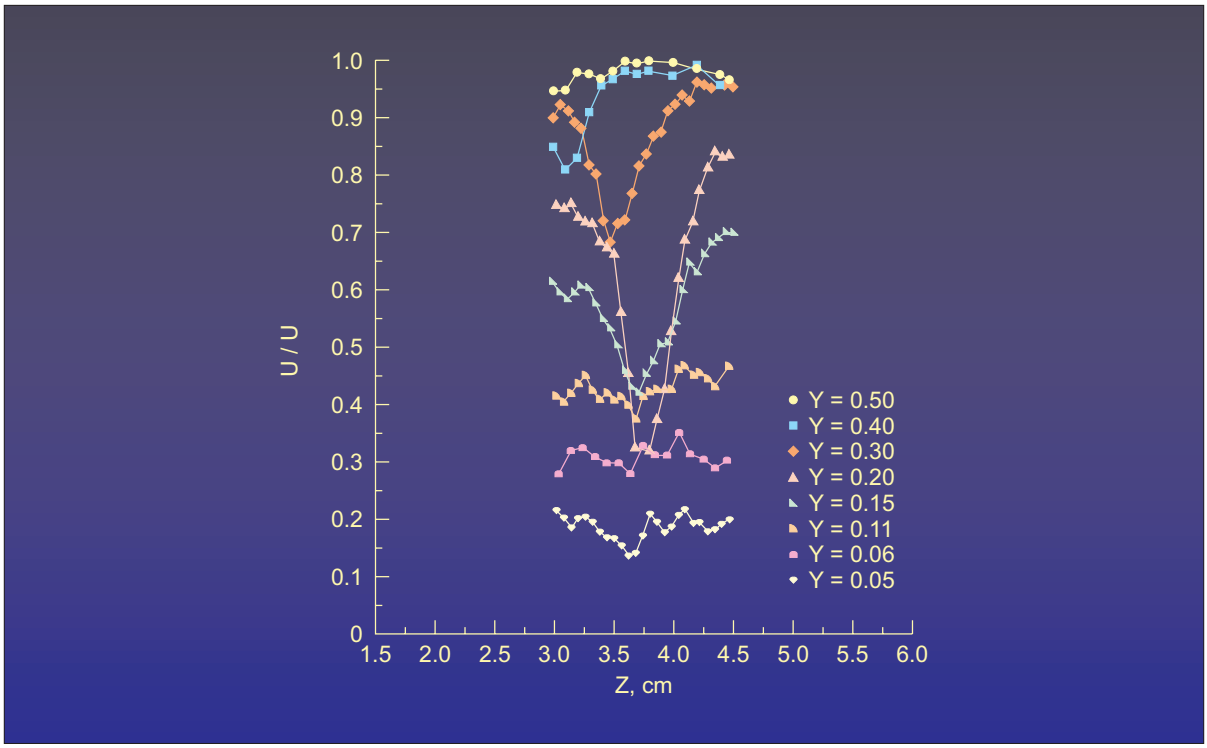

Figure 6(d).- Spanwise variation of streamwise velocity component $R_c = 2.1 \times 10^6$, $M_\infty = 0.05$, $G = 36.0$, $x/c = 0.225$.

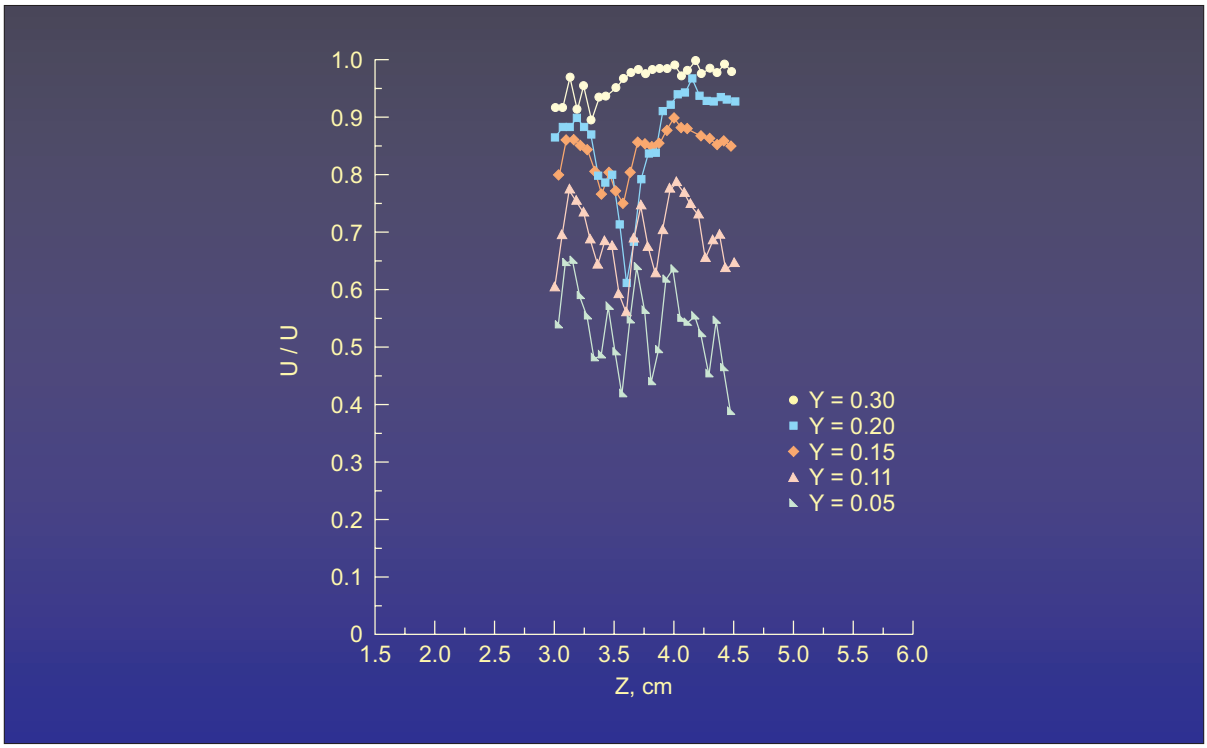

Figure 6(e).- Spanwise variation of streamwise velocity component $R_c = 2.1 \times 10^6$, $M_\infty = 0.05$, $G = 36.0$, $x/c = 0.25$.

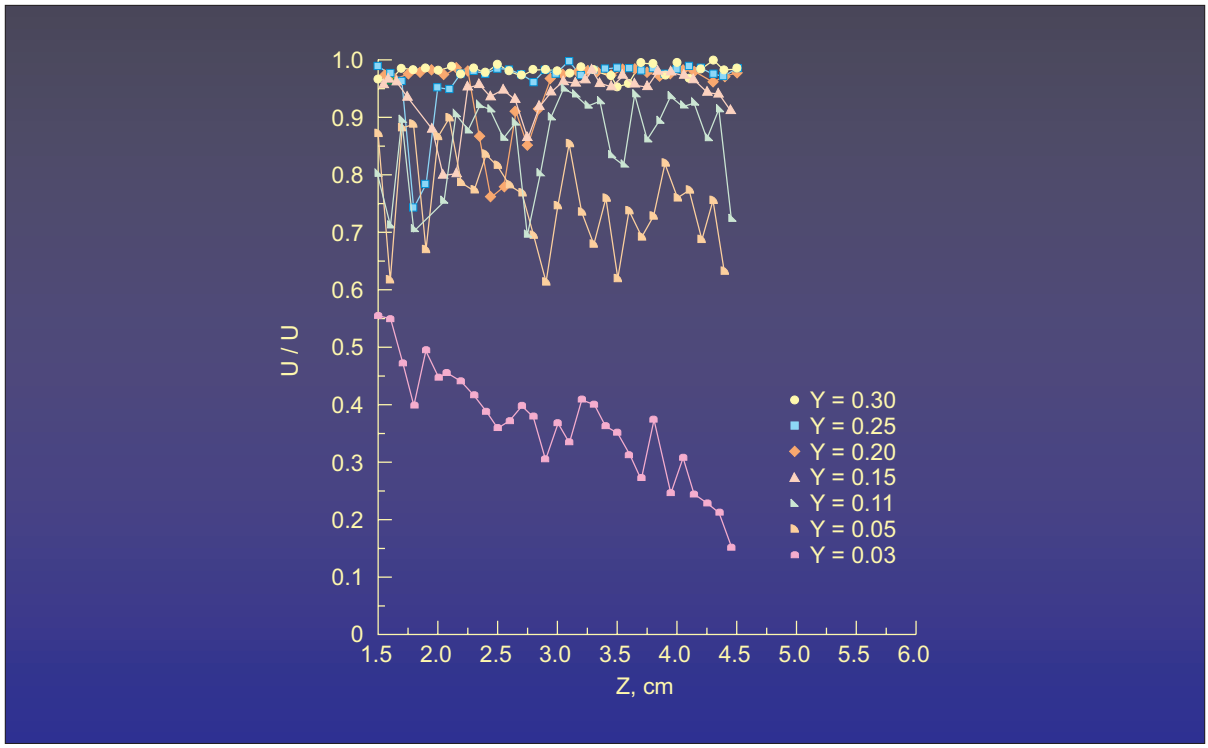

Figure 6(f).- Spanwise variation of streamwise velocity component $R_c = 2.1 \times 10^6$, $M_\infty = 0.05$, $G = 36.0$, $x/c = 0.275$.

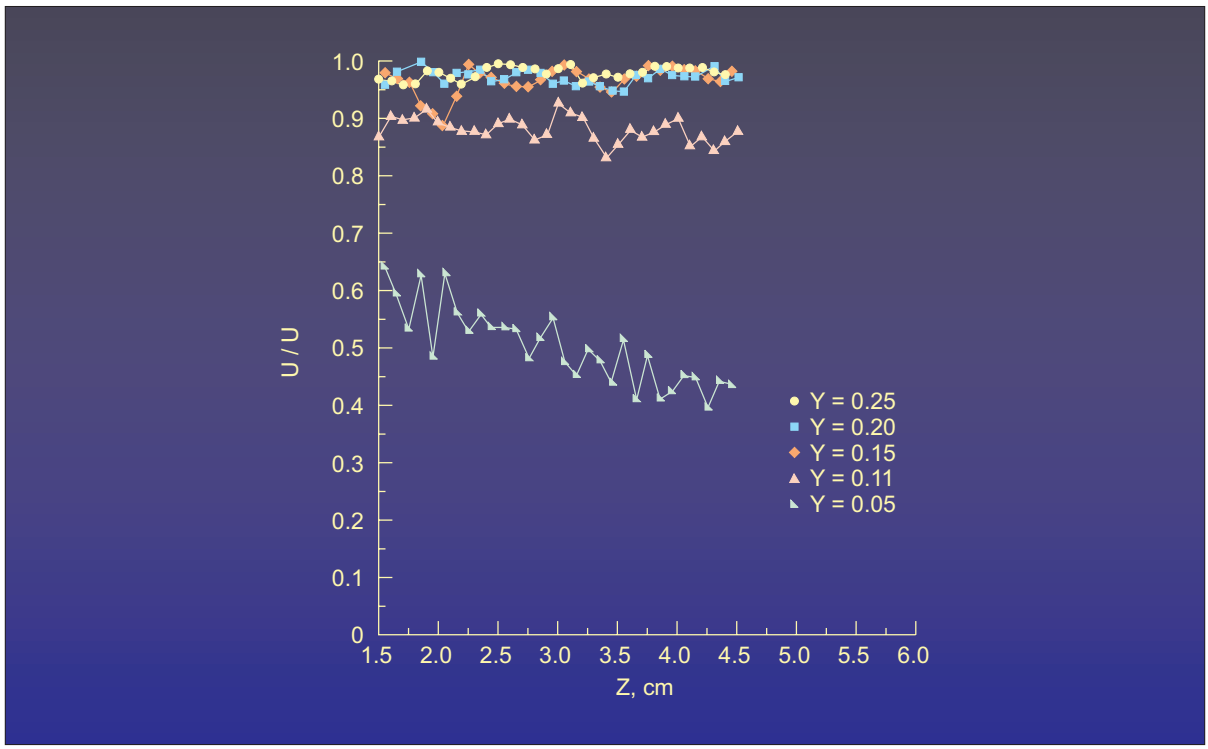

Figure 6(g).- Spanwise variation of streamwise velocity component $R_c = 2.1 \times 10^6$, $M_\infty = 0.05$, $G = 36.0$, $x/c = 0.30$.

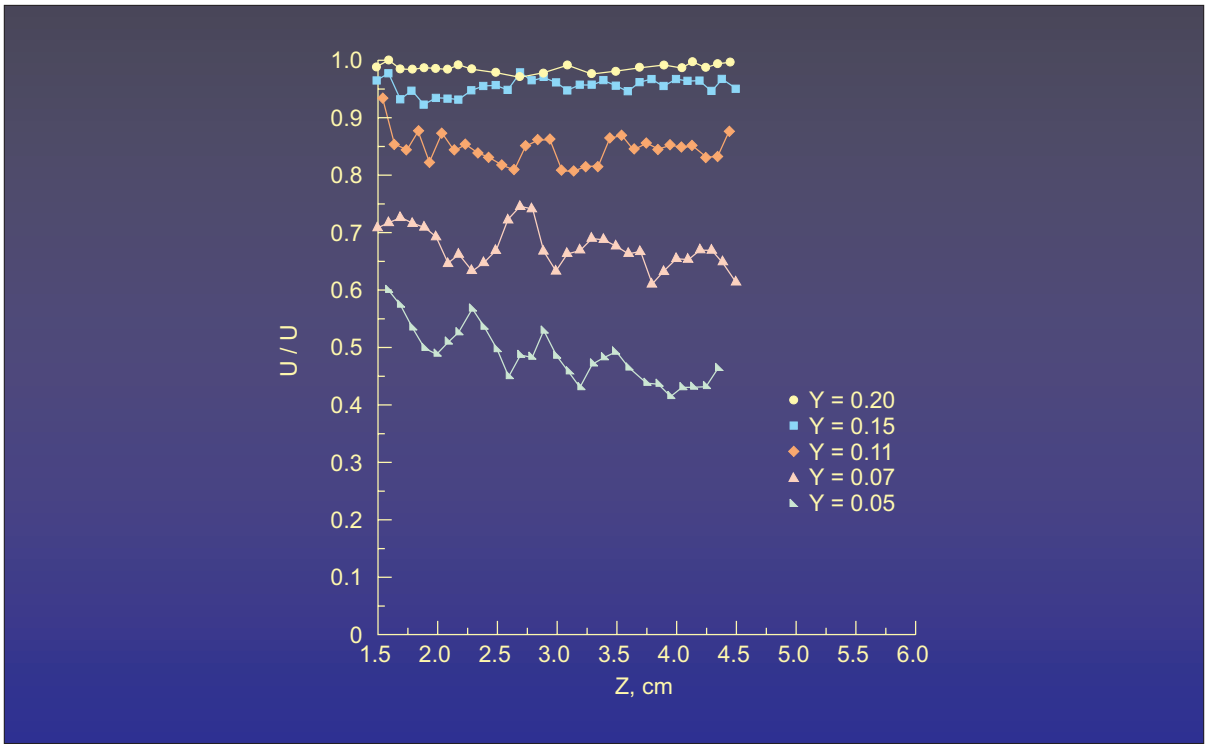

Figure 6(h).- Spanwise variation of streamwise velocity component $R_c = 2.1 \times 10^6$, $M_\infty = 0.05$, $G = 36.0$, $x/c = 0.3375$.

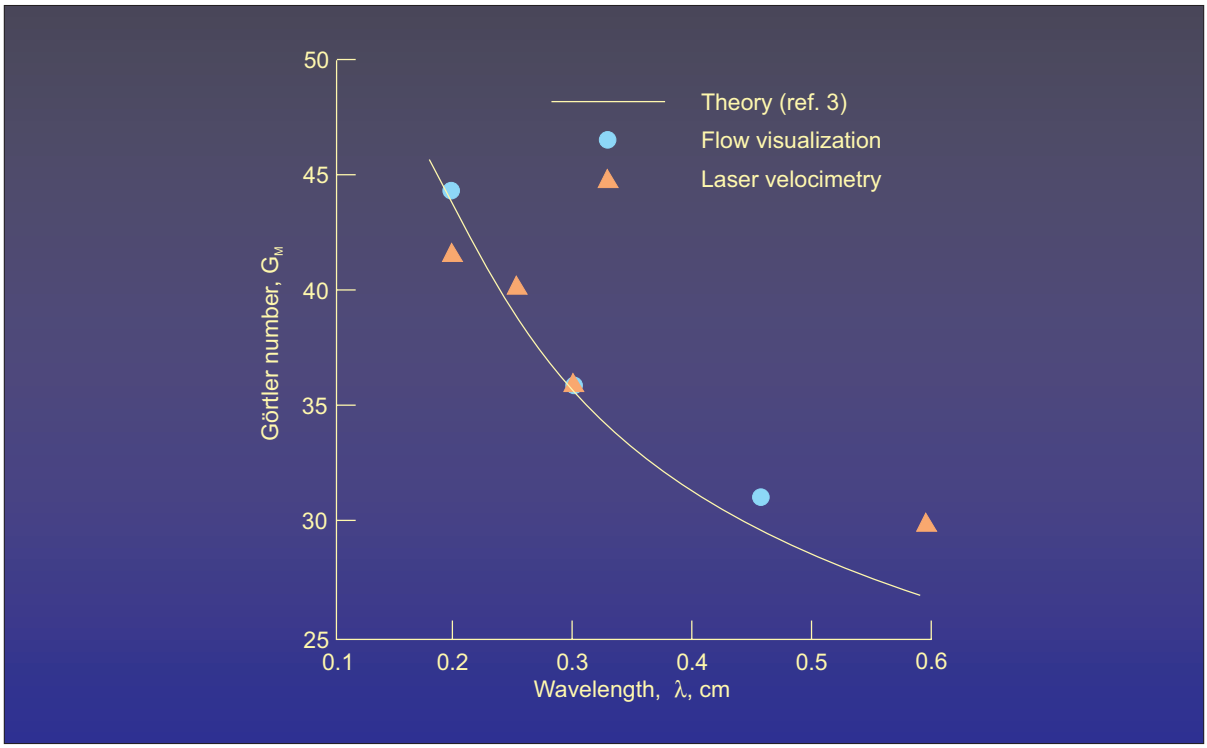

Figure 7.- Variation of dimensional wavelength with Görtler number, comparison with theory.

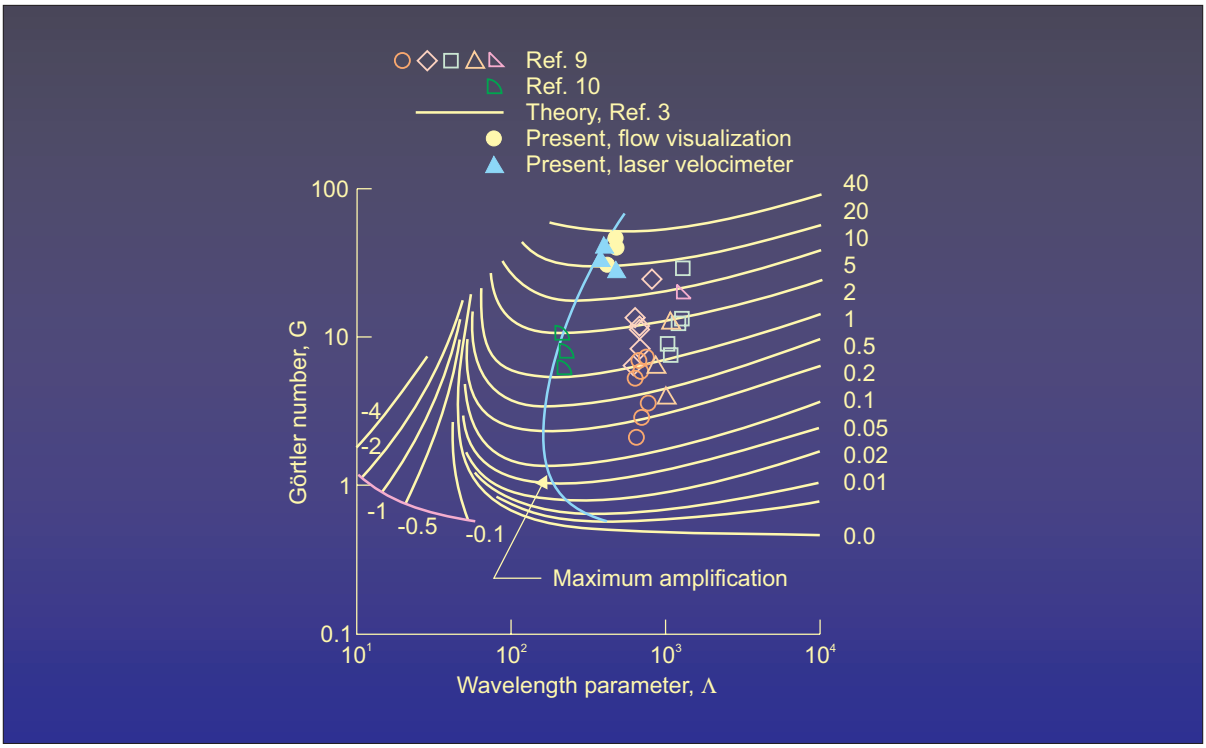

Figure 8.- Variation of nondimensional wavelength parameter with Görtler number, comparison with theory and other experiments.